

## Substituted 2-[(4-Aminomethyl)phenoxy]-2-methylpropionic Acid PPAR $\alpha$ Agonists. 1. Discovery of a Novel Series of Potent HDLc Raising Agents

Michael L. Sierra,<sup>†,‡</sup> Véronique Beneton,<sup>§</sup> Anne-Bénédict Boullay,<sup>||</sup> Thierry Boyer,<sup>‡</sup> Andrew G. Brewster,<sup>‡</sup> Frédéric Donche,<sup>‡</sup> Marie-Claire Forest,<sup>||</sup> Marie-Hélène Fouchet,<sup>‡</sup> Françoise J. Gellibert,<sup>‡</sup> Didier A. Grillot,<sup>||</sup> Millard H. Lambert,<sup>⊥</sup> Alain Laroze,<sup>‡</sup> Christelle Le Grumelec,<sup>‡</sup> Jean Michel Linget,<sup>§,¶</sup> Valerie G. Montana,<sup>⊥</sup> Van-Loc Nguyen,<sup>‡</sup> Edwige Nicodème,<sup>||</sup> Vipul Patel,<sup>⊗</sup> Annie Penfornis,<sup>‡</sup> Olivier Pineau,<sup>‡</sup> Danig Pohin,<sup>‡</sup> Florent Potvain,<sup>||</sup> Géraldine Poulain,<sup>‡,¶</sup> Cécile Bertho Ruault,<sup>‡</sup> Michael Saunders,<sup>||,⊙</sup> Jérôme Toum,<sup>‡</sup> H. Eric Xu,<sup>⊥,⊕</sup> Robert X. Xu,<sup>⊥</sup> and Pascal M. Pianetti<sup>\*,‡,§</sup>

Department of Medicinal Chemistry, Department of Biology, Department of Drug Metabolism and Pharmacokinetics, Laboratoire GlaxoSmithKline, Centre de Recherches, 25-27 avenue du Québec, 91951 Les Ulis, France, Department of Medicinal Chemistry, GlaxoSmithKline Research and Development, Medicines Research Centre, Gunnels Wood Road, Stevenage, Hertfordshire, SG1 2N7, United Kingdom, and Department of Computational, Analytical and Structural Sciences, GlaxoSmithKline, 5 Moore Drive, Research Triangle Park, North Carolina 27709

Received December 5, 2005

The peroxisome proliferator activated receptors PPAR $\alpha$ , PPAR $\gamma$ , and PPAR $\delta$  are ligand-activated transcription factors that play a key role in lipid homeostasis. The fibrates raise circulating levels of high-density lipoprotein cholesterol and lower levels of triglycerides in part through their activity as PPAR $\alpha$  agonists; however, the low potency and restricted selectivity of the fibrates may limit their efficacy, and it would be desirable to develop more potent and selective PPAR $\alpha$  agonists. Modification of the selective PPAR $\delta$  agonist **1** (GW501516) so as to incorporate the 2-aryl-2-methylpropionic acid group of the fibrates led to a marked shift in potency and selectivity toward PPAR $\alpha$  agonism. Optimization of the series gave **25a**, which shows EC<sub>50</sub> = 4 nM on PPAR $\alpha$  and at least 500-fold selectivity versus PPAR $\delta$  and PPAR $\gamma$ . Compound **25a** (GW590735) has been progressed to clinical trials for the treatment of diseases of lipid imbalance.

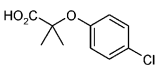
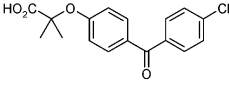
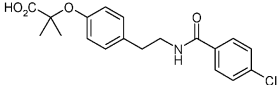
### Introduction

Elevated circulating levels of low-density lipoprotein cholesterol (LDLc) constitutes a major risk factor for coronary artery disease, and there exists a wealth of clinical data supporting the use of the LDLc-lowering statins in an increasingly wide range of patients.<sup>1</sup> More recently, the roles of both low circulating levels of high-density lipoprotein cholesterol (HDLc) and high circulating levels of triglycerides (TG) as cardiovascular disease risk factors have come into focus, and there is a growing level of confidence in the potential of drugs that lower TG or raise HDLc to play an important part in future cardiovascular drug therapy.<sup>2</sup>

The principal agents in current use for raising HDLc and lowering TG are the fibrates and nicotinic acid. The fibrates give increases of up to 20% in HDLc and decreases in TG of up to 40%;<sup>2,3</sup> nicotinic acid shows similar efficacy on HDLc with perhaps a slightly less pronounced effect on TG. It would be highly desirable to discover drugs that exert greater effects on HDLc and TG levels.

While the molecular target of nicotinic acid has only recently been identified,<sup>4</sup> the fibrates have been known for several years

**Table 1.** Human PPAR $\alpha$  Agonist Potencies of Fibrates<sup>a</sup>

Drug	Structure (active metabolite)	PPAR $\alpha$ EC <sub>50</sub> ( $\mu$ M)
Clofibrate		55
Fenofibrate		30
Bezafibrate		50

<sup>a</sup> Data were taken from ref 10 and were generated using the PPAR-GAL4 transactivation assay.

to act as agonists at the peroxisome proliferator activated receptor alpha (PPAR $\alpha$ ).<sup>5,6</sup> The PPARs comprise a family of ligand-activated transcription factors that play a key role in lipid homeostasis. There are three members of the family: PPAR $\alpha$ , PPAR $\delta$  (or  $\beta$ ), and PPAR $\gamma$ .<sup>7</sup> PPAR $\alpha$  is highly expressed in the liver, heart, and muscle and includes a range of fatty acids among its natural ligands. In man, activation of PPAR $\alpha$  results in increased clearance of TG-rich very low-density lipoprotein (VLDL) via a reduction in plasma levels of ApoCIII<sup>8</sup> and in upregulation of ApoA1, the principal lipoprotein component of HDL.<sup>9</sup> As a consequence, the fibrates lower TG and raise HDLc levels. The fibrates are only weakly potent PPAR $\alpha$  agonists,<sup>10</sup> as shown in Table 1. It has been proposed that more potent and subtype-selective PPAR $\alpha$  activators might offer enhanced specificity and reduced side effects compared with that of existing fibrates,<sup>11</sup> and several groups have reported the

\* To whom correspondence should be addressed. Tel.: (33) 1 69 29 60 05. Fax : (33) 1 69 07 48 92. E-mail : pascal.m.pianetti@gsk.com.

<sup>†</sup> Current address: Leo Pharma AS, 55 Industriparken, DK-2750 Ballerup, Denmark.

<sup>‡</sup> Department of Medicinal Chemistry, Les Ulis.

<sup>§</sup> Department of Drug Metabolism and Pharmacokinetics.

<sup>||</sup> Department of Biology.

<sup>⊥</sup> Computational, Analytical and Structural Sciences.

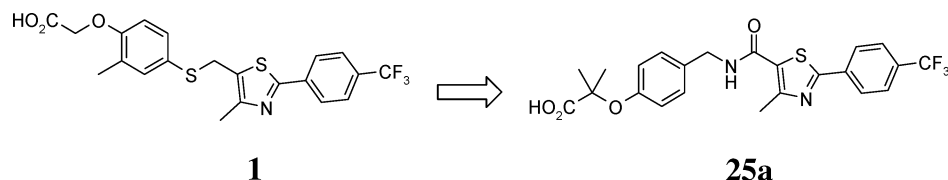
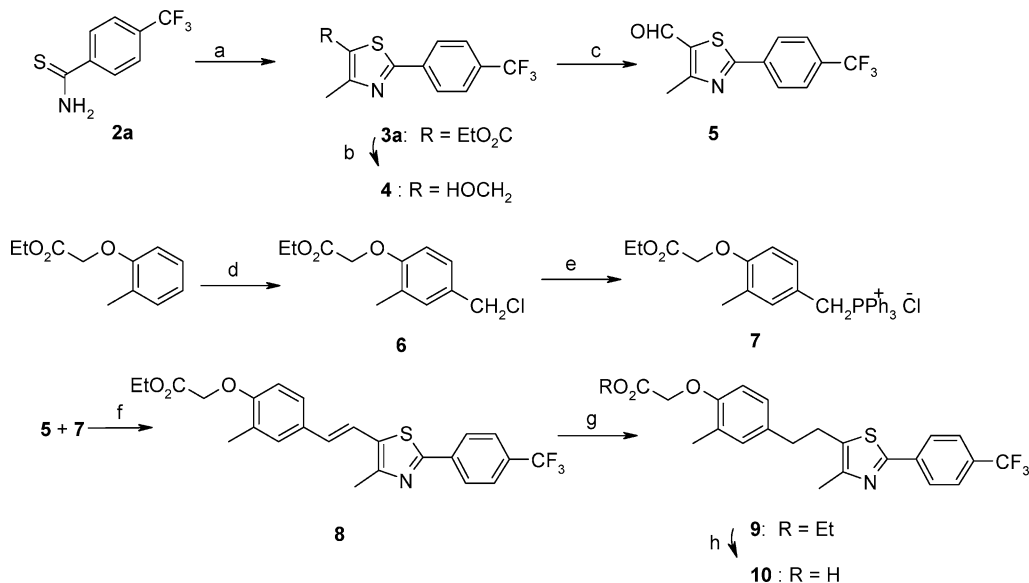
<sup>¶</sup> Current address : CareX, Bd Sebastien Brant, BP 30442, 47412 ILLKIRCH Cedex.

<sup>⊗</sup> Department of Medicinal Chemistry, Stevenage.

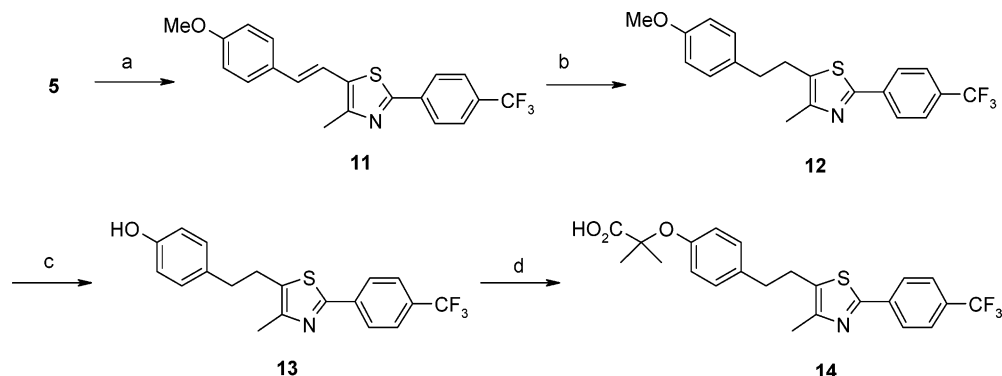
<sup>⊙</sup> Current address : Bio-Michs sprl, 132 rue Berkendael, 1050 Bruxelles, Belgium.

<sup>⊕</sup> Current address : Laboratory of Structural Sciences, Van Andel Research Institute, 333 Bostwick Avenue, Grand Rapids, MI 49503.

## Scheme 1

Scheme 2<sup>a</sup>

<sup>a</sup> Reagents and conditions: (a) ethyl-2-chloroacetoacetate, EtOH, reflux; (b) LiAlH<sub>4</sub>, THF, 0 °C; (c) PCC, CH<sub>2</sub>Cl<sub>2</sub>, rt; (d) conc. HCl, petroleum ether, 37% HCHO/H<sub>2</sub>O; (e) PPh<sub>3</sub>, toluene, reflux; (f) NaH (60% in mineral oil), anhydrous EtOH, rt; (g) 10% Pd/C, EtOH/dioxane, H<sub>2</sub>; (h) NaOH (1 N), dioxane, reflux.

Scheme 3<sup>a</sup>

<sup>a</sup> Reagents and conditions: (a) 4-methoxybenzyltriphenylphosphonium chloride, NaH (60% in mineral oil), CH<sub>2</sub>Cl<sub>2</sub>; (b) 10% Pd/C, EtOH/AcOH, H<sub>2</sub>; (c) BBr<sub>3</sub>, CH<sub>2</sub>Cl<sub>2</sub>, -40 °C; (d) 2-trichloromethyl-2-propanol, acetone, NaOH (conc), rt.

discovery of potent PPAR $\alpha$  agonists and their effects in animal models of dyslipidemia.<sup>12</sup>

We describe below how, starting from the recently published<sup>13</sup> selective PPAR $\delta$  agonist **1** (GW501516) which showed weak potency on PPAR $\alpha$ , we have first incorporated the classical fibrate “head group” to improve selectivity for PPAR $\alpha$  and subsequently optimized potency and selectivity. We have thus developed a new series of highly potent and selective PPAR $\alpha$  agonists, one of which, **25a**, is currently in clinical trials for the treatment of dyslipidemia (Scheme 1).

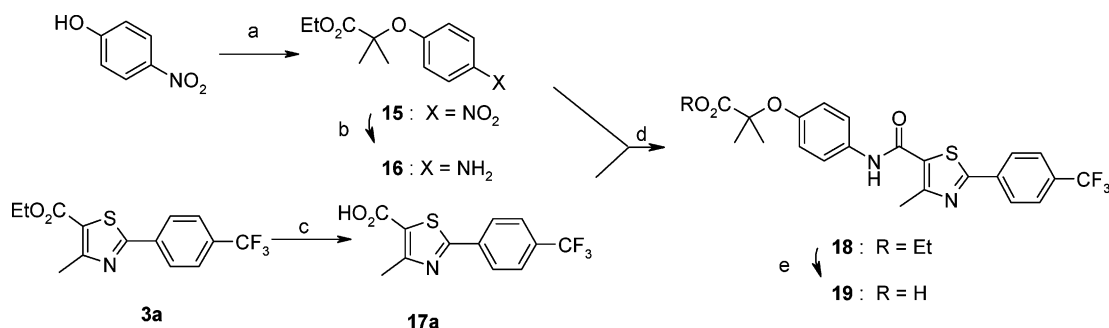
## Chemistry

Compound **10** was prepared as shown in Scheme 2. Condensation of 4-trifluoromethylthiobenzamide **2a** with ethyl-2-chloroacetoacetate gave the thiazole **3a**, which was reduced with

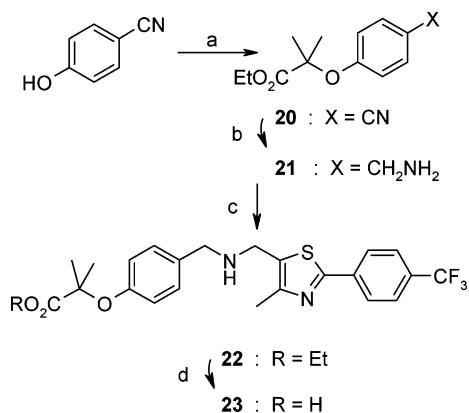
LiAlH<sub>4</sub> and oxidized with PCC to give the aldehyde **5**. Compound **7** was prepared in two steps from ethyl 2-methylphenoxyacetate via reaction with formaldehyde and HCl to give **6** followed by substitution with triphenylphosphine to give **7**. Wittig condensation of **5** with **7** gave the alkene **8**, which was hydrogenated over 10% Pd on carbon to give **9**. Hydrolysis using NaOH in dioxane furnished compound **10**.

Compound **14** was synthesized according to the procedure depicted in Scheme 3. Wittig condensation of **5** with 4-methoxybenzyltriphenylphosphonium chloride gave **11**, which was hydrogenated over 10% Pd on carbon to give **12**. Demethylation using boron tribromide gave **13**, and coupling with 2-trichloromethyl-2-propanol and hydrolysis afforded **14**.

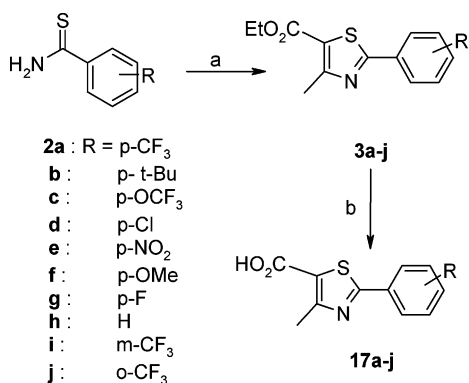
Alkylation of 4-nitrophenol followed by hydrogenolysis gave **16**, which was coupled with the acid **17a**, prepared by hydrolysis

Scheme 4<sup>a</sup>

<sup>a</sup> Reagents and conditions: (a) ethyl 2-bromo-2-methylpropanoate, DMF, K<sub>2</sub>CO<sub>3</sub>, 40 °C; (b) 5% Pd/C, EtOH, 30 °C, H<sub>2</sub>; (c) NaOH (aq), EtOH, reflux; (d) HOBT, EDC, Et<sub>3</sub>N, DMF, rt; (e) NaOH (1 N), EtOH, 40 °C.

Scheme 5<sup>a</sup>

<sup>a</sup> Reagents and conditions: (a) NaH (60% in mineral oil), DMF, ethyl-2-bromo-2-methylpropanoate, rt then reflux; (b) 10% Pd/C, AcOH/EtOH, H<sub>2</sub>; (c) 5, NaBH(OAc)<sub>3</sub>, dichloroethane/AcOH, rt; (d) NaOH (1 N), EtOH, 40 °C.

Scheme 6<sup>a</sup>

<sup>a</sup> Reagents and conditions: (a) ethyl-2-chloroacetoacetate, EtOH, reflux; (b) NaOH (1 N), EtOH, reflux.

of ester **3a**, to give **18**. Hydrolysis using NaOH in EtOH gave **19**, as shown in Scheme 4.

Compound **23** was prepared from 4-cyanophenol via alkylation and hydrogenation to give **21**, which was reacted with aldehyde **5** under reductive amination conditions. The standard hydrolysis gave **23** (Scheme 5).

Thiazole carboxylic acids **17b–j** were prepared in the same manner as **17a**, as indicated in Scheme 6. The acids **17a–j** were then elaborated to the amides **25a–j** via coupling using either HOBT/EDC/Et<sub>3</sub>N or SOCl<sub>2</sub>, followed by hydrolysis (Scheme 7).

*N*-Methylamide **27** was obtained by methylation of **24a** using NaH and methyl iodide followed by hydrolysis, as shown in Scheme 8.

The reversed amide **34** was prepared as shown in Scheme 9. Bromination of **4** using PBr<sub>3</sub> gave **28**. Substitution by potassium phthalimide gave **29**, which was cleaved by hydrazine to give the amine **30**. Compound **30** was coupled with **32**, in turn prepared by alkylation of 4-hydroxybenzaldehyde followed by oxidation using sodium chlorite and sodium hydrogen phosphate, giving **33**, which was then hydrolyzed to give **34**.

The homologated amide **37** was synthesized via HOBT coupling of **17a** with 4-hydroxyphenethylamine followed by alkylation and hydrolysis, as shown in Scheme 10.

Compound **25k** was prepared by hydrogenolysis of **24e** followed by hydrolysis (Scheme 11).

The 4-methanesulfonyloxy thiazole carboxylic ester **31** was prepared from 4-hydroxythiobenzamide **2k** using the procedure described above, followed by mesylation using methane sulfonyl chloride and triethylamine. LiOH mediated hydrolysis gave the carboxylic acid **17k**, which was alkylated to give ester **24l**. Hydrolysis under mild conditions (1 equiv of LiOH, rt) of **24l** gave product **25l**, whereas more vigorous hydrolysis of **24l** (NaOH, THF/EtOH, 70 °C) gave the phenol **25m** (Scheme 12).

The regioisomeric thiazole **41** was prepared in a similar manner to **25a** via the carboxylic acid **39**, obtained from condensation of **2a** in refluxing ethanol with the intermediate obtained from the reaction of 2-ketobutyric acid with bromine to give **38**, followed by hydrolysis. Coupling of **39** with **21** followed by standard hydrolysis gave **41**, as depicted in Scheme 13.

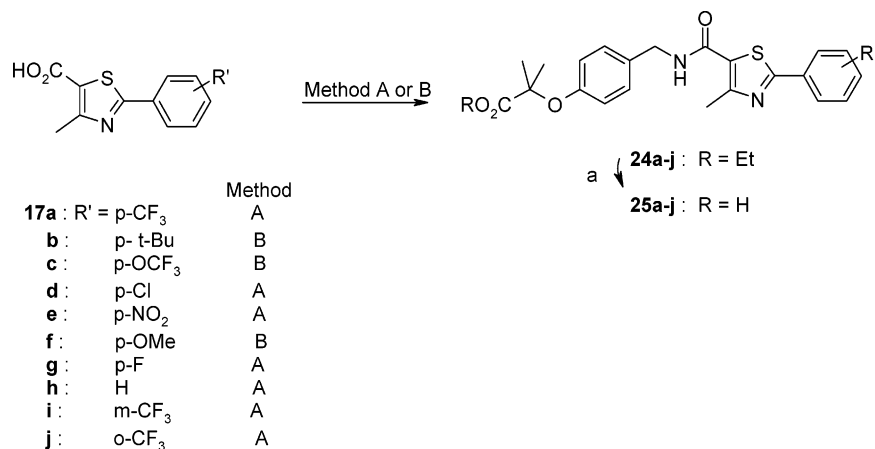
The trifluoromethyl-substituted thiazole **45** was prepared using a similar route to that used for **25a**, substituting ethyl-2-chloro-4,4,4-trifluoroacetate for the methyl analogue (Scheme 14).

## Results and Discussion

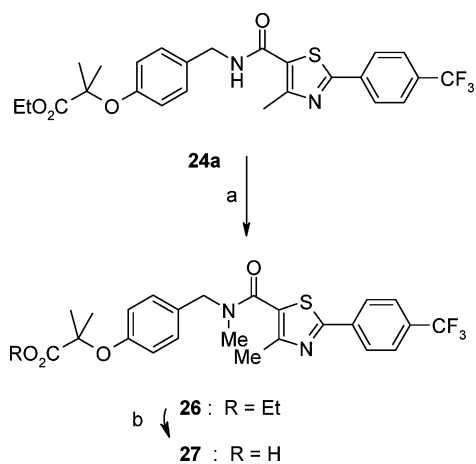
The recently published **1** is a potent agonist at PPAR $\delta$  with around 1000-fold selectivity with respect to PPAR $\alpha$ , as measured using cell-based transient-transfection assays<sup>14</sup> (Table 2).

Replacement of the thiomethylene chain of **1** by ethylene gave **10**, which showed equally low potency against PPAR $\alpha$ . PPAR $\delta$  potency was somewhat decreased (EC<sub>50</sub> = 4 nM) relative to **1**, while PPAR $\gamma$  activity remained very weak. Encouragingly however, replacement of the *o*-methyl phenoxyacetate group by the classical “fibrate head group” shared by all of the drugs shown in Table 1 gave **14**, which regained potency against PPAR $\alpha$  (EC<sub>50</sub> = 210 nM).

We further explored the effect of modifying the chain linking the head group to the biaryl unit (Table 3). Replacement of the ethylene of **14** by an amide link gave **19**, which showed almost complete loss of activity. However, increasing the length of the linking chain proved beneficial for PPAR $\alpha$  potency. The

Scheme 7<sup>a</sup>

<sup>a</sup> Reagents and conditions: Method A, SOCl<sub>2</sub>, **21**, Et<sub>3</sub>N, CH<sub>2</sub>Cl<sub>2</sub>; Method B, **21**, HOBT, EDC, Et<sub>3</sub>N, DMF, rt; (a) NaOH (1 N), THF, reflux.

Scheme 8<sup>a</sup>

<sup>a</sup> Reagents and conditions: (a) NaH (60% in mineral oil), MeI, DMF, 40 °C; (b) NaOH (1 N), EtOH, reflux.

methyleneaminomethylene derivative **23** gained 3-fold in potency, and the amide **25a** showed a 50-fold increase in potency. *N*-Methylation (**27**) of the amide **25a** was detrimental to PPAR $\alpha$  potency, and the inverse amide **34** and the chain-extended amide **37** were also less potent.

Replacement of the terminal trifluoromethyl substituent by a range of groups showed that substitution in this position was largely well tolerated and that potency correlated well with the lipophilicity of the substituent (Table 4). Thus the *tert*-butyl, trifluoromethyl, and trifluoromethoxy groups gave the highest potency, while fluoro, hydrogen, and amino substituents gave a progressive decrease in potency. All compounds demonstrated considerable selectivity for PPAR $\alpha$ .

The *m*-trifluoromethyl analogue **25i** was equipotent with **25a** versus PPAR $\alpha$ , whereas the *o*-trifluoromethyl analogue **25j** lost both PPAR $\alpha$  potency and selectivity versus PPAR $\delta$ . The *p*-hydroxy **25m** and *p*-methanesulfonyloxy **25l** substituted compounds were inactive.

We next investigated the effect of modifying the central heterocycle fragment (Table 5). The thiazole regioisomer **41** showed a 500-fold decrease in PPAR $\alpha$  potency compared with **25a**, whereas PPAR $\delta$  potency increased. The trifluoromethyl analogue **45** showed similar PPAR $\alpha$  agonist potency to that of **25a** but was less selective versus PPAR $\gamma$ .

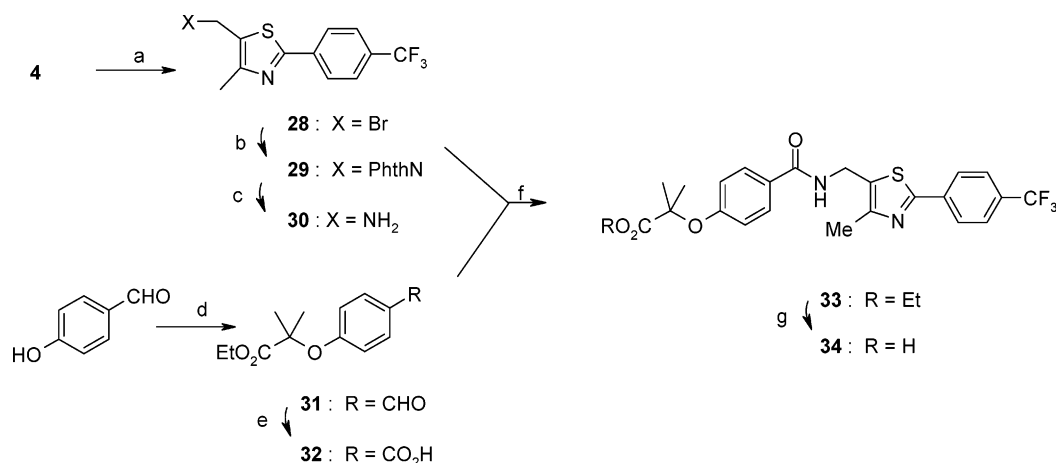
**Binding Mode of 25a in the PPAR $\alpha$  Ligand Binding Domain.** To determine with precision the binding mode of this new series of ligands, **25a** was cocrystallized with PPAR $\alpha$ . As

shown in Figure 1, **25a** fits well into the PPAR $\alpha$  binding site. The carboxylate moiety of the head group forms four hydrogen bonds with Ser-280, Tyr-314, Tyr-464, and His-440, as expected from the previous PPAR $\alpha$  X-ray crystal structures of GW409544<sup>15</sup> and AZ242.<sup>16</sup> The gem-dimethyl substituents are directed into a lipophilic pocket bounded by Phe-273, Gln-277, Val-444, and Leu-456, a region at the top end of the so-called "benzophenone" pocket.<sup>17</sup> These residues are conserved in PPAR $\gamma$  and PPAR $\delta$  except for Val-444, which is leucine in PPAR $\gamma$  and methionine in PPAR $\delta$ . This side chain is smallest and most able to accommodate the fibrate headgroup in PPAR $\alpha$  and is largest and least able to accommodate the fibrate headgroup, in PPAR $\delta$ .<sup>14,18</sup> This might explain why **14** gains potency versus PPAR $\alpha$  and PPAR $\gamma$  while maintaining a similar level of PPAR $\delta$  potency compared with **10**.

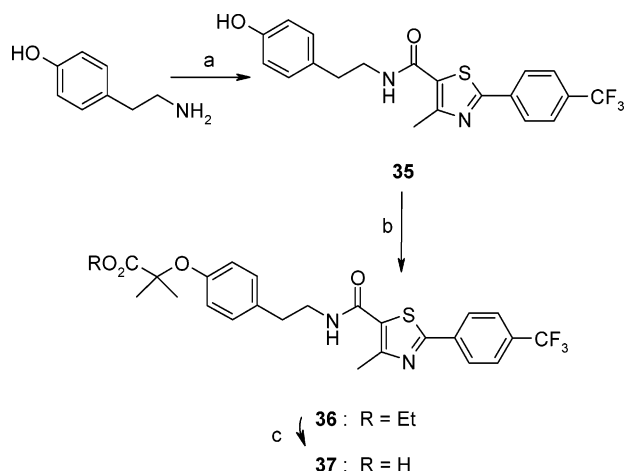
The amide group of **25a** adopts a *trans*-conformation in which the carbonyl group of **25a** adopts a *trans*-conformation in which the carbonyl oxygen is directed toward Thr-279 and nearby water molecules. Although the carbonyl oxygen of **25a** lies near Thr-279, the threonine side chain appears to adopt a conformation that turns its hydroxyl group away from the carbonyl oxygen. Instead of hydrogen bonding with this threonine, the carbonyl oxygen hydrogen bonds indirectly with Ser-280 and Thr-283 via two water molecules (Figure 2a). Thr-279 is hydrogen bonded to the backbone NH of Ala-333 via a third water molecule and oriented toward the sulfur of the thiazole in a manner likely to give a favorable interaction, even though sulfur does not form strong hydrogen bonds.

The amide NH is positioned close to the methyl group of the thiazole and surrounded by three sulfur-containing amino acids, Cys-276, Met-355, and Met-330, with the sulfur atoms directed toward the NH proton at distances of 4.38 Å, 2.92 Å, and 3.33 Å, respectively (Figure 2b). This relatively polar environment stabilizes the partial positive charge of the NH, thereby favoring the observed conformation of **25a**. Overall, the linking amide group of **25a** appears to be well stabilized by the protein environment with the carbonyl surrounded by a very strong hydrogen bond network and the NH by a triad of polar atoms. This remarkable environment might explain the potency and selectivity of the amide linker compound in the PPAR $\alpha$  pocket, which is more lipophilic and less solvent-exposed than the corresponding pockets of either PPAR $\gamma$  or PPAR $\delta$ .<sup>15</sup>

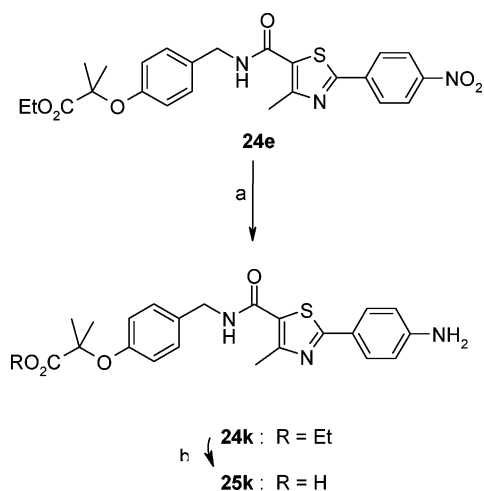
The precise binding network around the amide linker might also account for the observation that any modification resulted in a decrease in PPAR $\alpha$  potency. *N*-Methylation in **27** is not well tolerated due to the proximity of the sulfur atoms, and the reverse amide of **34** binds less favorably because its carbonyl

Scheme 9<sup>a</sup>

<sup>a</sup> Reagents and conditions: (a) PBr<sub>3</sub>, CH<sub>2</sub>Cl<sub>2</sub>, 0 °C; (b) potassium phthalimide, DMF, 70 °C; (c) hydrazine hydrate, EtOH, 90 °C; (d) ethyl-2-bromo-2-methylpropanoate, K<sub>2</sub>CO<sub>3</sub>, DMF, 40 °C; (e) NaClO<sub>2</sub>, NaHPO<sub>3</sub>, H<sub>2</sub>O, *t*-BuOH, rt; (f) SOCl<sub>2</sub>, Et<sub>3</sub>N, CH<sub>2</sub>Cl<sub>2</sub>; (g) NaOH (1 N), THF, reflux.

Scheme 10<sup>a</sup>

<sup>a</sup> Reagents and conditions: (a) **17a**, HOBT, EDC, DMF, Et<sub>3</sub>N, rt; (b) ethyl-2-bromo-2-methylpropanoate, K<sub>2</sub>CO<sub>3</sub>, DMF, 80 °C; (c) NaOH (1 N), THF, reflux.

Scheme 11<sup>a</sup>

<sup>a</sup> Reagents and conditions: (a) 10% Pd/C, EtOH, rt; (b) NaOH (1 N), THF, reflux.

oxygen is probably not hydrogen bonded and is instead surrounded by three lipophilic amino acids.

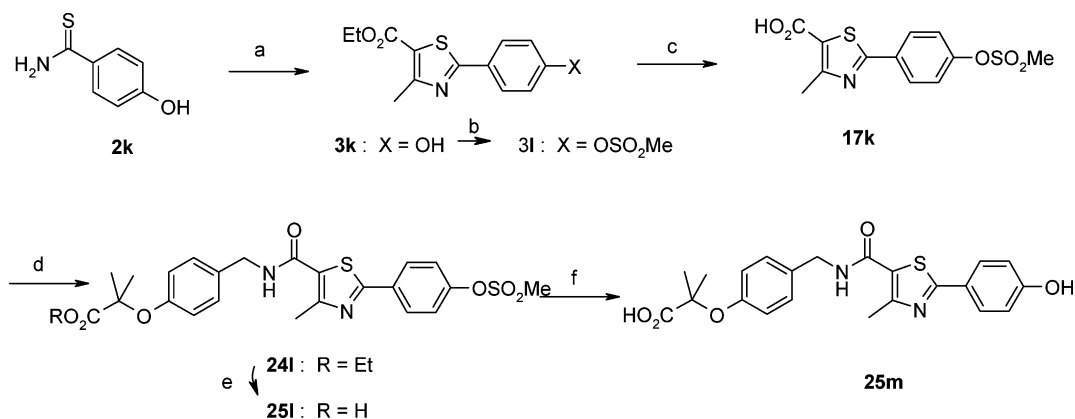
The nitrogen atom of the thiazole ring is not involved in any discernible interaction with the binding site, whereas the methyl

group fits well into a pocket that is connected with the bottom end of the benzophenone pocket. This pocket is bounded by Cys-276, Met-330, Leu-344, and Met-355 residues, which are conserved in PPAR $\gamma$  and PPAR $\delta$  with the exception of Met-330, which is valine in PPAR $\gamma$  and leucine in PPAR $\delta$ , and Met-355, which is isoleucine in PPAR $\delta$ . The smaller valine side-chain in PPAR $\gamma$  could accommodate slightly larger substituents at this position on the thiazole, while the branched isoleucine in PPAR $\delta$  might crowd larger substituents. In accordance with this hypothesis, replacement of the methyl by a trifluoromethyl group in **45** maintains PPAR $\alpha$  but increases PPAR $\gamma$  potency and decreases PPAR $\delta$  potency.

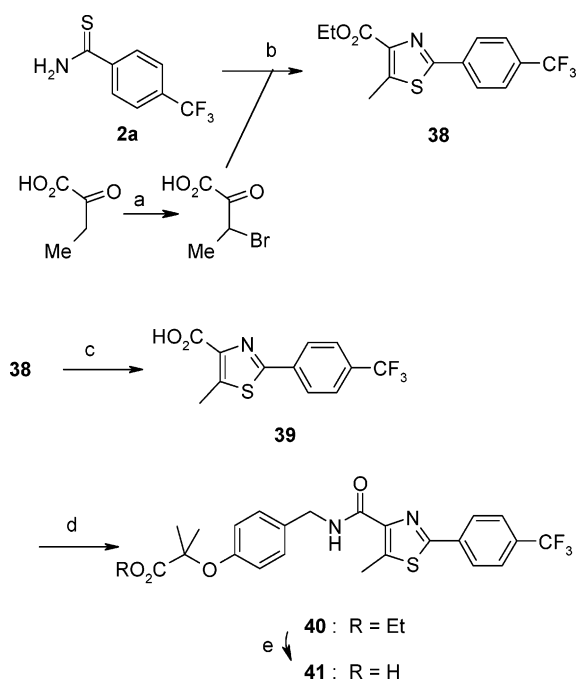
The phenyl-trifluoromethyl moiety makes a good fit into the lower pocket of the binding site and would be expected to contribute favorably to overall binding through van der Waals interactions. This observation is compatible with SAR data that show a relationship between size and lipophilicity of the *para*-substituent and PPAR $\alpha$  potency. The decrease in potency seen with compounds bearing polar *para*-substituents (**25k** and **25m**) may be explained by the hydrophobic nature of the lower pocket. The inactivity of the methylsulfonyl analogue **25i** may be due to a combination of polarity and steric constraints. *meta*-Substitution is well tolerated as evidenced by the fact that **25i** is equipotent with **25a**. Although the X-ray structure of **25a** shows that one *meta*-position is directed toward Leu-247 and Ile-241, the other *meta*-position points into an open space and could easily accept a substituent. On the other hand, *ortho*-substitution would force the phenyl group out of plane with the thiazole and likely lead to a clash with the wall of the narrow pocket, a conjecture that is consistent with the decrease in potency seen with **25j**.

**Pharmacokinetics in Rat and Dog (Table 6).** Following intravenous administration of compound **25a** (2.7 mg/kg) to the rat, distribution to the tissues was limited with the volume of distribution (1 L/kg) similar to that of total body water (0.6 L/kg). Total plasma clearance was low (5 mL/min/kg), representing about 6% of rat hepatic blood flow. The low clearance and moderate volume of distribution resulted in a plasma half-life of 2.4 h. Following a single oral dose of compound **25a** at 3 mg/kg, the maximum concentration of compound in the plasma was 1461 ng/mL after 1.5 h. The bioavailability was high (47%).

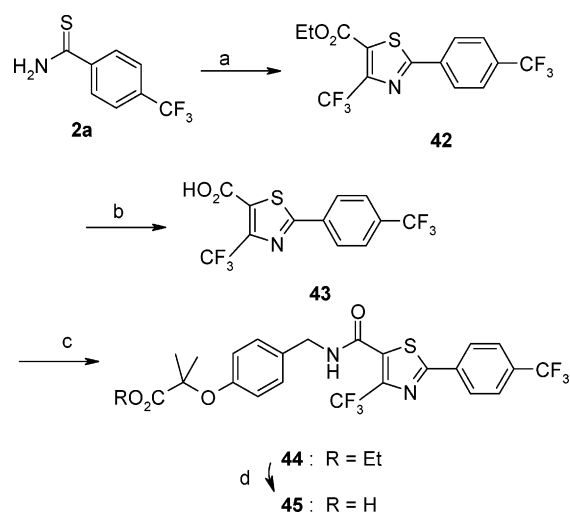
Following intravenous administration of compound **25a** to the dog at 2 mg/kg, distribution to the tissues was limited with the volume of distribution (2.8 L/kg) being greater than that of

Scheme 12<sup>a</sup>

<sup>a</sup> Reagents and conditions: (a) ethyl-2-chloroacetoacetate, EtOH, reflux; (b) MeSO<sub>2</sub>Cl, Et<sub>3</sub>N, toluene/acetone; (c) LiOH (1.5 equiv), rt; (d) **21**, HOBT, EDC, DMF, Et<sub>3</sub>N, rt; (e) LiOH (1 equiv), THF/H<sub>2</sub>O, rt; (f) NaOH (1 N), EtOH, THF, 70°.

Scheme 13<sup>a</sup>

<sup>a</sup> Reagents and conditions: (a) Br<sub>2</sub>; (b) EtOH, reflux; (c) NaOH (1 N), EtOH, reflux; (d) **21**, HOBT, EDC, DMF, Et<sub>3</sub>N, rt; (e) NaOH (1 N), THF, reflux.

Scheme 14<sup>a</sup>

<sup>a</sup> Reagents and conditions: (a) ethyl-2-chloro-4,4,4-trifluoroacetoacetate, DMF, 100 °C; (b) LiOH (1 N), EtOH, rt; (c) SOCl<sub>2</sub>, **21**, NEt<sub>3</sub>, CH<sub>2</sub>Cl<sub>2</sub>; (d) NaOH (1 N), THF, reflux.

Table 2

compd	1 : X = S 10 : X = CH <sub>2</sub>		14
	PPARα <sup>a</sup> EC <sub>50</sub> <sup>b</sup> (μM) (% activation) <sup>b,c</sup>	PPARδ <sup>a</sup> EC <sub>50</sub> <sup>b</sup> (μM) (% activation) <sup>b,c</sup>	PPARγ <sup>a</sup> EC <sub>50</sub> <sup>b</sup> (μM) (% activation) <sup>b,c</sup>
<b>1</b>	1.888 ± 0.1 (108 ± 1%)	0.001 ± 0.000 09 (97 ± 1%)	8.900 ± 0.27 (80 ± 1%)
<b>10</b>	2.0 <sup>d</sup> (85%)	0.004 <sup>d</sup> (117%)	10.0 <sup>d</sup> (74%)
<b>14</b>	0.21 ± 0.08 (138 ± 61%)	0.02 ± 0.07 (90 ± 10%)	1.87 ± 0.79 (76 ± 14.9%)

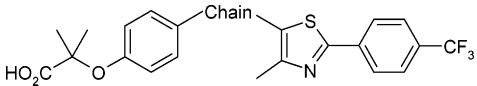
<sup>a</sup> Data generated using cell based transient transfection assays described in ref 13. <sup>b</sup> ±SD. <sup>c</sup> Percent of maximal activation of all compounds was compared to reference compounds normalized to 100%. For the PPARα activity, the reference compound was **25a**. For the PPARδ and PPARγ activities, the reference compounds were **1** and rosiglitazone, respectively. <sup>d</sup> Results of a single experiment.

total body water (0.6 L/kg). Total plasma clearance was moderate (13 mL/min/kg), representing about 35% of hepatic blood flow in the dog. The moderate clearance and low volume of distribution resulted in a plasma half-life of 2.6 h. Following a single oral dose of compound **25a** at 3 mg/kg, the maximum concentration of compound in the plasma was 1449 ng/mL. The bioavailability was high (85%).

**In Vivo Pharmacology.** Several compounds in this series demonstrated profound in vivo activity in animal models of dyslipidemia, as illustrated by compound **25a**. The human Apo-A-I-transgenic mouse model has been proposed to be potentially relevant to human disease, because in this model, fibrates give upregulation rather than the repression of Apo-A-I seen in other rodent models.<sup>19</sup> Compound **25a** shows similar PPARα agonist potency and selectivity versus murine and human PPARs (murine PPAR EC<sub>50</sub>, α = 15 nM; δ = 1000 nM; γ > 10 000 nM). When administered orally twice a day for 5 days, **25a**, prepared as a suspension in 0.5% HPMC 100/1% Tween80 at pH = 7.0, gave dose-related decreases in circulating TG,

VLDLc, and LDLc and concomitant increases in HDLc (Table 7). The ED<sub>50</sub> for the HDL effect was approximately 1 mg/kg. Circulating levels of Apo-A-I were also increased by the

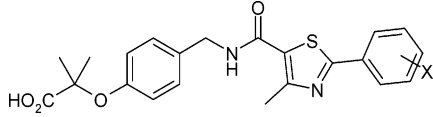
Table 3



cmpd	chain	PPAR $\alpha^a$	PPAR $\delta^a$	PPAR $\gamma^a$
		EC $_{50}^b$ ( $\mu$ M) (% activation) <sup>b,c</sup>	EC $_{50}^b$ ( $\mu$ M) (% activation) <sup>b,c</sup>	EC $_{50}^b$ ( $\mu$ M) (% activation) <sup>b,c</sup>
14	–CH <sub>2</sub> CH <sub>2</sub> –	0.21 $\pm$ 0.08 (138 $\pm$ 61%)	0.02 $\pm$ 0.07 (90 $\pm$ 10%)	1.87 $\pm$ 0.79 (76 $\pm$ 14.9%)
19	–NHCO–	9.5 $\pm$ 0.5 (69 $\pm$ 0%)	> 10	> 10
23	–CH <sub>2</sub> NHCH <sub>2</sub> –	0.07 $\pm$ 0.01 (110 $\pm$ 4%)	4.05 $\pm$ 1.1 (61 $\pm$ 2%)	> 10
25a	–CH <sub>2</sub> NHCO–	0.004 $\pm$ 0.002 (95 $\pm$ 14%)	2.83 $\pm$ 1.18 (82 $\pm$ 21%)	> 10
27	–CH <sub>2</sub> NMeCO–	0.24 <sup>d</sup> (84%)	> 10	> 10
34	–CONHCH <sub>2</sub> –	1.32 <sup>d</sup> (109%)	6.26 <sup>d</sup> (62%)	> 10
37	–CH <sub>2</sub> CH <sub>2</sub> NHCO–	0.11 $\pm$ 0.05 (129 $\pm$ 58%)	> 10	> 10

<sup>a</sup> Data generated using cell based transient transfection assays described in ref 13. <sup>b</sup>  $\pm$ SD. <sup>c</sup> Percent of maximal activation of all compounds was compared to reference compounds normalized to 100%. For the PPAR $\alpha$  activity, the reference compound was **25a**. For the PPAR $\delta$  and PPAR $\gamma$  activities, the reference compounds were **1** and rosiglitazone, respectively. <sup>d</sup> Results of a single experiment.

Table 4

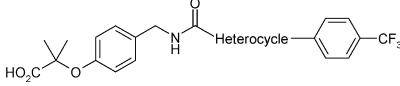


cmpd	X	PPAR $\alpha^a$	PPAR $\delta^a$	PPAR $\gamma^a$
		EC $_{50}^b$ ( $\mu$ M) (% activation) <sup>b,c</sup>	EC $_{50}^b$ ( $\mu$ M) (% activation) <sup>b,c</sup>	EC $_{50}^b$ ( $\mu$ M) (% activation) <sup>b,c</sup>
25a	<i>p</i> -CF <sub>3</sub>	0.004 $\pm$ 0.002 (95 $\pm$ 14%)	2.83 $\pm$ 1.18 (82 $\pm$ 21%)	> 10
25b	<i>p</i> - <i>t</i> -butyl	0.005 $\pm$ 0.000 (66 $\pm$ 6%)	> 10	0.86 $\pm$ 0.01 (78 $\pm$ 0%)
25c	<i>p</i> -OCF <sub>3</sub>	0.004 $\pm$ 0.000 (116 $\pm$ 5%)	4.6 $\pm$ 0.5 (73 $\pm$ 3%)	> 10
25d	<i>p</i> -Cl	0.01 $\pm$ 0.003 (94 $\pm$ 7%)	5.4 $\pm$ 0.9 (85 $\pm$ 9%)	> 10
25e	<i>p</i> -NO <sub>2</sub>	0.03 $\pm$ 0.01 (111 $\pm$ 17%)	> 10	> 10
25f	<i>p</i> -OMe	0.01 $\pm$ 0.01 (103 $\pm$ 8%)	> 10	> 10
25g	<i>p</i> -F	0.04 <sup>d</sup> (118%)	> 10	> 10
25h	H	0.12 $\pm$ 0.02 (107 $\pm$ 5%)	> 10	> 10
25i	<i>m</i> -CF <sub>3</sub>	0.004 <sup>d</sup> (106%)	> 25	> 25
25j	<i>o</i> -CF <sub>3</sub>	0.465 <sup>d</sup> (82%)	0.808 <sup>d</sup> (74%)	> 25
25k	<i>p</i> -NH <sub>2</sub>	5.64 $\pm$ 0.29 (67 $\pm$ 4%)	> 10	> 10
25l	<i>p</i> -OSO <sub>2</sub> Me	> 10	> 10	> 10
25m	<i>p</i> -OH	> 10	> 10	> 10

<sup>a</sup> Data generated using cell based transient transfection assays described in ref. 13. <sup>b</sup>  $\pm$ SD. <sup>c</sup> Percent of maximal activation of all compounds was compared to reference compounds normalized to 100%. For the PPAR $\alpha$  activity, the reference compound was **25a**. For the PPAR $\delta$  and PPAR $\gamma$  activities, the reference compounds were **1** and rosiglitazone, respectively. <sup>d</sup> Results of a single experiment.

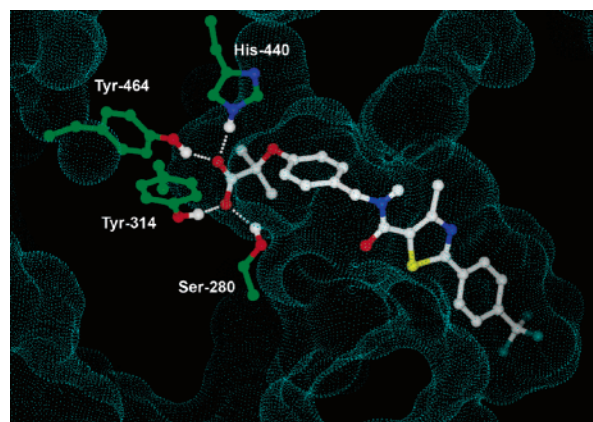
treatment (data not shown), consistent with the mechanism of action. As a reference, Fenofibrate was tested in human Apo-A-I transgenic mice at 50 mg/kg. It produced the expected profile with a decrease in plasma TG (–43%), VLDL cholesterol (–64%), and LDL cholesterol (–78%), as well as an increase

Table 5



#	Heterocycle	PPAR $\alpha^a$	PPAR $\delta^a$	PPAR $\gamma^a$
		EC $_{50}$ ( $\mu$ M) <sup>b</sup> (%activation) <sup>b,c</sup>	EC $_{50}$ ( $\mu$ M) <sup>b</sup> (%activation) <sup>b,c</sup>	EC $_{50}$ ( $\mu$ M) <sup>b</sup> (%activation) <sup>b,c</sup>
25a		0.004 $\pm$ 0.002 (95 $\pm$ 14%)	2.83 $\pm$ 1.18 (82 $\pm$ 21%)	>10
41		1.89 <sup>d</sup> (171%)	0.66 <sup>d</sup> (103%)	>10
45		0.004 $\pm$ 0.002 (98 $\pm$ 8%)	8.24 $\pm$ 1.75 (54 $\pm$ 5%)	0.73 $\pm$ 0.12 (63 $\pm$ 1%)

<sup>a</sup> Data generated using cell based transient transfection assays described in ref 13. <sup>b</sup>  $\pm$ SD. <sup>c</sup> Percent of maximal activation of all compounds was compared to reference compounds normalized to 100%. For the PPAR $\alpha$  activity, the reference compound was **25a**. For the PPAR $\delta$  and PPAR $\gamma$  activities, the reference compounds were **1** and rosiglitazone, respectively. <sup>d</sup> Results of a single experiment.



**Figure 1.** X-ray crystal structure of **25a** complexed with the PPAR $\alpha$  ligand binding domain. The molecular surface of the binding site is represented by blue dots. Interactions of the head group amino acids with the carboxylate moiety of the ligand are shown as white dotted lines. The hydrogens shown here and in Figure 2a,b were not visible in the electron density and were instead positioned to optimize their hydrogen bonding interactions.

in HDL cholesterol (+26%). The finding that **25a** is able to lower LDLc and TG and increase HDL cholesterol in the Apo-A-I-transgenic mouse model suggests that it will deliver significant therapeutic benefit in the treatment of dyslipidemia and hypertriglyceridemia. Compound **25a** (GW590735) has been progressed to clinical trials for the treatment of diseases of lipid imbalance.

## Conclusions

Starting from the selective PPAR $\delta$  agonist **1**, which showed weak potency on PPAR $\alpha$ , we have developed a new series of highly potent and selective PPAR $\alpha$  agonists, one of which, **25a**, has progressed to clinical evaluation. The superior potency and PPAR subtype selectivity of **25a** suggest that this compound offers the potential to deliver significantly improved therapeutic benefits over the fibrates in dyslipidemia and hypertriglyceridemia.

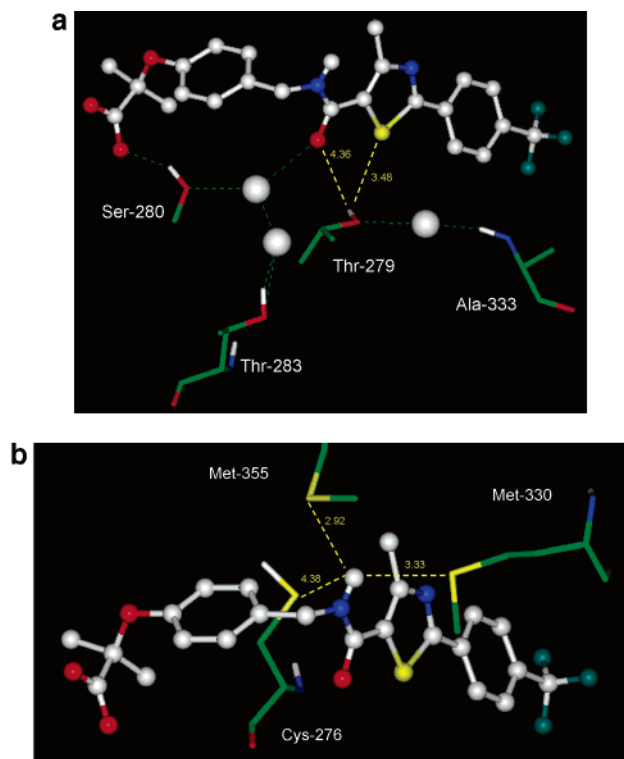


**Figure 2.** (a) Environment of the linking amide group of **25a**: hydrogen bond network surrounding the carbonyl. Water molecules are shown as white spheres; hydrogen bond interactions are represented as green dotted lines; distances are indicated in Å and represented as yellow dotted lines; for clarity of the figure, the amino acid backbone was deleted for Ser-280 and Thr-279. (b) Environment of the linking amide group of **25a**: triad of sulfur containing amino acids surrounding the amide NH. NH-S distances are indicated in Å and represented as yellow dotted lines.

**Table 6.** Pharmacokinetic Data for Compound **25a**

PK parameter	rat	dog
Cl (mL/min/kg)	5	13
Vd (L/kg)	1	2.8
$T_{1/2}$ (h)	2.4	2.6
F (%)	47	85

**Table 7.** Effect of **25a** in the Human Apo-A-I Transgenic Mouse Model<sup>a</sup>

oral dose (mg/kg, b.i.d.)	VLDL chol (g/L) %	LDL chol (g/L) %	HDL chol (g/L) %	TG (g/L) %
0.5	-48 ± 8	-61 ± 2	+43 ± 4	-37 ± 6
1.0	-63 ± 10	-65 ± 3	+51 ± 19	-48 ± 11
5.0	-86 ± 5	-69 ± 5	+86 ± 18	-65 ± 6

<sup>a</sup> All changes are statistically significant ( $p < 0.05$ ), as determined by one-way ANOVA analysis.

## Experimental Section

**General Methods.** All commercial chemicals and solvents are reagent grade and were used without further purification unless otherwise specified. All reactions except those in aqueous media were carried out with the use of standard techniques for the exclusion of moisture. Reactions were monitored by thin-layer chromatography on 0.25 mm silica gel plates (60F-254, E. Merck) and visualized with UV light or 5% phosphomolybdic acid in 95% ethanol.

Final compounds were typically purified either by flash chromatography on silica gel (E. Merck, 40–63 mm) or by recrystallization. <sup>1</sup>H NMR spectra were recorded on either a Bruker 300 MHz Avance DPX or a Bruker 400 MHz Avance DRX instrument. Chemical shifts are reported in parts per million (ppm,  $\delta$  units).

Splitting patterns are designed as s, singlet; d, doublet; t, triplet; q, quartet; m, multiplet; bs, broad singlet. Low-resolution mass spectra (MS) were recorded on a Micromass platform LC or a Agilent GC/MS spectrometer. High-resolution mass spectra were recorded on a Micromass LCT (TOF) spectrometer. Mass spectra were acquired in either positive or negative ion mode under electrospray ionization (ESI) or atmospheric pressure chemical ionization (APCI) methods.

Analytical high performance liquid chromatography (HPLC; system A) was conducted on a Chromolith Performance RP 18 column (100 × 4.6 mm id) eluting with 0.01 M ammonium acetate in water and 100% acetonitrile (CH<sub>3</sub>CN), using the following elution gradient: 0 to 100% CH<sub>3</sub>CN over 4 min and 100% CH<sub>3</sub>CN over 1 min at 5 mL/min at a temperature of 30 °C.

Analytical HPLC (system B) was conducted on a XTERRA-MS C18 column (30 × 3 mm id, 2.5  $\mu$ m) eluting with 0.01 M ammonium acetate in water and 100% acetonitrile (CH<sub>3</sub>CN), using the following elution gradient: 0 to 100% CH<sub>3</sub>CN over 4 min and 100% CH<sub>3</sub>CN over 1 min at 1.1 mL/min at a temperature of 40 °C.

Analytical HPLC (system C) was conducted on a Uptisphere-hsc column (3  $\mu$ m 33 × 3 mm id) eluting with 0.01 M ammonium acetate in water and 100% acetonitrile (CH<sub>3</sub>CN) using the following elution gradient: 0–5% CH<sub>3</sub>CN over 0.5 min, gradient 5–100% CH<sub>3</sub>CN over 3.25 min, and 100% CH<sub>3</sub>CN over 0.75 min at 1.3 mL/min at a temperature of 40 °C.

Analytical HPLC (system D) was conducted on a Uptisphere-hsc column (3  $\mu$ m 33 × 3 mm id) eluting with 0.01 M ammonium acetate in water and 100% acetonitrile (CH<sub>3</sub>CN) using the following elution gradient: 0–5% CH<sub>3</sub>CN over 0.5 min, gradient 5–100% CH<sub>3</sub>CN over 6.25 min, and 100% CH<sub>3</sub>CN over 0.75 min at 1.3 mL/min at a temperature of 40 °C.

The purity of key compounds was determined on two analytic HPLC systems using UV detection.

**Pharmacokinetics in Rat and Dog.** Compound **25a** was administered to Wistar rats ( $n = 15$ ) by oral gavage at dose of 3 mg/kg in pH 7 buffer, 0.1% Tween80 and by intravenous injection via the penis vein ( $n = 30$ ) at a dose of 2.7 mg/kg in 10% DMSO and PEG200. Compound **25a** was administered orally to male beagle dogs ( $n = 3$ ) by stomach intubation at a dose of 3 mg/kg in pH 7 buffer, 0.1% Tween80 and by intravenous injection via the cephalic vein at a dose of 2 mg/kg in 10% DMSO and PEG200. Blood samples were placed on wet ice, and plasma was collected after centrifugation. Plasma samples were stored frozen at -20 °C until time of analysis. Plasma samples (0.5 mL) were diluted with 1:1 buffer (NaH<sub>2</sub>PO<sub>4</sub>, 0.1 M, pH 4) and then extracted with ethyl acetate (5 mL). The ethyl acetate was evaporated, and the residue was resuspended in 200  $\mu$ L of mobile phase (water/acetonitrile/TFA; 30v/70v/0.1%). Samples were analyzed by high-performance liquid chromatography spectrometric analysis (LC/MS/MS). Pharmacokinetic parameters were determined by SIPHAR.

**Apo-A-I Transgenic Mouse Model.** Male C57BL/6 mice transgenic for human ApoA-I were obtained from Charles River Laboratories (L'Arbresle, France) and randomized into treatment groups of  $n = 5$  animals. Twice a day oral administration of vehicle (0.5% HPMC/1% Tween80, pH = 7.0) or indicated doses of compound as a suspension began when animals were nine weeks old and lasted for 5 days. Animals were fasted overnight before blood samples were taken by intracardiac puncture. Whole liver was collected and weighed. Blood samples were left for 30 min at 37 °C to coagulate and centrifuged 10 min at 10 000 rpm. Total serum fraction was then collected and frozen at -20 °C until use. Total cholesterol and total TG were dosed using kits 61219 and 61236, respectively, following manufacturer instructions (Bio Mérieux, Marcy-l'Étoile, France). After 10 min of incubation at 37 °C, the colorimetric reaction was read at 492 nm with an iEMS reader (ThermoLife Sciences, Cergy-Pontoise, France). Cholesterol HDL, LDL, and VLDL fractions were separated by HPLC. Samples were diluted 1/5 in phosphate buffer (Ca<sup>++</sup> and Mg<sup>-</sup> free) and filtered on 0.45  $\mu$ m to remove excess proteins before HPLC. All changes reported with an asterisk are statistically significant ( $p < 0.05$ ) as determined by one-way ANOVA analysis.

**Chemicals. Substituted Thiobenzamides 2a-j.** Substituted thiobenzamides were either purchased from commercial suppliers (**2a**, **2d**, **2f**, **2h** Lancaster; **2c** Fluorochem; **2g** Acros) or were prepared using one of the routes **a** or **b** described below.

**Procedure a for the Preparation of 2b.** To a solution of  $P_4S_{10}$  (0.2 mmol) in toluene (100 mL) was added  $NaHCO_3$  (2 mmol), and the mixture was heated to reflux for about 30 min. The substituted benzamide (1 mmol) was added, and the reaction was stirred at 90 °C for 1 h. The reaction was then evaporated to dryness, treated with brine (100 mL), and extracted with  $CH_2Cl_2$  (2 × 50 mL). The organic phase was dried, filtered, and evaporated to afford the final product. In this manner were obtained products **2b** (orange solid; 49%).  $^1H$  NMR ( $CDCl_3$ ):  $\delta$  7.7 (d, 2H), 7.4 (bs, 1H), 7.3 (d, 2H), 7.0 (bs, 1H), 1.2 (s, 9H).

**Procedure b for the Preparation of Substituted Thiobenzamides 2e, 2i, and 2j.** To the substituted benzonitrile (1 mmol) in DMF (30 mL) was added dropwise DMF (21 mL) saturated with  $HCl_{(g)}$  over a period of 1 min. Thioacetamide (2 mmol) was then added, and the reaction was heated to 100 °C for 1 h.  $HCl_{(g)}$  was bubbled in for about 1 min, and stirring was continued at 100 °C for another 18 h. The reaction was cooled to rt, treated with ice, and extracted with  $Et_2O$  (3 × 250 mL). The organic phase was washed with  $H_2O$  (3 × 300 mL), dried over  $Na_2SO_4$ , filtered, and evaporated to dryness. The residue was washed with a mixture of isopropyl ether/pentane (1:3) to afford the final product. In this manner were obtained products **2e** (orange solid; 83%),  $^1H$  NMR (DMSO- $d_6$ )  $\delta$  10.1 (bs, 1H), 9.7 (bs, 1H), 8.1 (d, 2H), 7.9 (d, 2H); **2i** (light yellow solid; 88%),  $^1H$  NMR (DMSO)  $\delta$  8.20 (bs, 1H), 8.08 (s, 1H), 8.02 (d,  $J=7.9$  Hz, 1H), 7.91 (d,  $J=7.9$  Hz, 1H), 7.76 (t,  $J=7.9$  Hz, 1H), 7.34 (bs, 1H); and **2j** (light yellow solid; 47%),  $^1H$  NMR (DMSO)  $\delta$  7.9–7.4 (m, 4H), 7.8 (bs, 1H), 7.06 (bs, 1H).

**Ethyl 4-Methyl-2-[4-(trifluoromethyl)phenyl]-1,3-thiazole-5-carboxylate (3a).** To a suspension of 4-(trifluoromethyl)-thiobenzamide **2a** (302.4 g, 1.47 mol) in ethyl alcohol (1.5 L, 5 vol) was added at room temperature ethyl 2-chloroacetoacetate (203.8 mL, 1 equiv). The solution was refluxed for 24 h, and then the solvent was removed under reduced pressure. The solid material was stirred with cooled hexane (500 mL) for 30 min, filtered, and washed with hexane (2 × 150 mL). Drying gave crude compound **3a** (352.9 g). A second crop of 25.7 g was obtained by concentration of the hexane filtrates to 50 mL, giving an overall yield of 378.6 g (81.5%).  $^1H$  NMR ( $CDCl_3$ ):  $\delta$  8.06 (d,  $J=8.1$  Hz, 2H), 7.69 (d,  $J=8.2$  Hz, 2H), 7.36 (q,  $J=7.1$  Hz, 2H), 2.78 (s, 3H), 1.39 (t,  $J=7.1$  Hz, 3H).

**4-Methyl-2-[4-(trifluoromethyl)phenyl]-1,3-thiazole-5-carboxylic Acid (17a).** To a cooled solution of **3a** (378.6 g, 1.2 mol) in ethyl alcohol (2 L, 5 vol) was added a solution of sodium hydroxide (96.15 g, 2 equiv) in 2 L of water. The solution was heated at 85 °C for 1.5 h. After evaporation of the ethyl alcohol, the aqueous solution was diluted with 2 L of water and acidified to pH = 1 with concentrated aqueous hydrochloric acid. The solid material was filtered and washed twice with 1 L of water and 1 L of dichloromethane. After drying in a vacuum oven, **17a** (267.2 g) was obtained as an off-white powder. A second crop of 25.7 g was obtained by concentration of the dichloromethane and triturating with pentane, giving an overall yield of **17a** of 292.9 g (85%).  $^1H$  NMR (DMSO- $d_6$ ):  $\delta$  13.51 (bs, 1H), 8.15 (d,  $J=8.3$  Hz, 2H), 7.84 (d,  $J=8.7$  Hz, 2H), 2.68 (s, 3H).

**2-Methyl-2-[4-[(4-methyl-2-[4-(trifluoromethyl)phenyl]thiazol-5-ylcarbonyl)amino]methyl]phenoxy]propionic Acid Ethyl Ester (24a).** A suspension of crude **17a** (38.7 g, 0.13 mol) in thionyl chloride (200 mL, 5 vol) was refluxed for 3 h. After return to room temperature, the thionyl chloride was removed under reduced pressure, and the residue was washed twice with toluene (100 mL) and evaporated to dryness. The crude acid chloride obtained (off-white solid) was used without purification. To a mixture of crude **21** (35.5 g; 1 equiv/LC-MS purity: 90%) and triethylamine (20.62 mL, 1.1 equiv) in dichloromethane (350 mL, 10 vol), maintained at 10 °C, was added portionwise the acid chloride over 20 min, and the mixture was stirred at room temperature overnight. The

reaction was quenched by addition of water (200 mL) and was stirred for 5 min. The aqueous layer was extracted with dichloromethane (2 × 200 mL). The combined organic layers were washed with hydrochloric acid (1 N, 200 mL), water (200 mL), saturated aqueous sodium carbonate (200 mL), and brine (200 mL). After drying over magnesium sulfate, filtration, and concentration to dryness, the crude material was suspended in isopropyl ether (200 mL), triturated, filtered, and dried to give **24a** (47.6 g, 69.7%) as a white powder:  $^1H$  NMR (DMSO- $d_6$ ):  $\delta$  8.87 (t,  $J=5.6$  Hz, 1H), 8.14 (d,  $J=8.1$  Hz, 2H), 7.87 (d,  $J=8.5$  Hz, 2H), 7.23 (d,  $J=8.7$  Hz, 2H), 6.75 (d,  $J=8.7$  Hz, 2H), 4.37 (d,  $J=5.8$  Hz, 2H), 4.15 (q,  $J=7.1$  Hz, 2H), 2.63 (s, 3H), 1.50 (s, 6H), 1.16 (t,  $J=7.1$  Hz, 3H).

**2-Methyl-2-[4-[(4-methyl-2-[4-(trifluoromethyl)phenyl]thiazol-5-ylcarbonyl)amino]methyl]phenoxy]propionic Acid (25a).** To a solution of **24a** (230.8 g, 0.46 mol) in 1.2 L (5 vol) of tetrahydrofuran was added aqueous sodium hydroxide (1 N, 480 mL, 1.05 equiv). The solution was stirred under reflux for 18 h. After removal of THF under reduced pressure, 1 N NaOH (500 mL) and methyl alcohol (100 mL) were added. The aqueous layer was extracted with dichloromethane (2 × 400 mL) and acidified to pH = 1 with concentrated aqueous hydrochloric acid. The oily residue was extracted with dichloromethane (3 × 400 mL), and the combined organic layers were washed with brine (600 mL). After drying over magnesium sulfate, filtration, and concentration to dryness, the oily residue was triturated with pentane (500 mL), filtered, and washed with pentane (2 × 250 mL) to give, after drying, crude compound **25a** (207.2 g) as a white powder. The solid material was dissolved in 310 mL (1.5 vol) of boiling toluene. After filtration of the hot solution and return to room temperature, the crystallized material was filtered, washed with toluene (2 × 200 mL), and dried in vacuo to give **25a** (196.3 g, 90%), as a white powder; mp 130–131 °C;  $^1H$  NMR (DMSO- $d_6$ )  $\delta$  13.0 (bs, 1H), 8.87 (t,  $J=5.7$  Hz, 1H), 8.14 (d,  $J=8.1$  Hz, 2H), 7.87 (d,  $J=8.3$  Hz, 2H), 7.22 (d,  $J=8.7$  Hz, 2H), 6.78 (d,  $J=8.7$  Hz, 2H), 4.37 (d,  $J=5.9$  Hz, 2H), 2.63 (s, 3H), 1.48 (s, 6H). MS (APCI)  $m/z$  479 (M + H)<sup>+</sup>. HRMS calcd for  $C_{23}H_{21}F_3N_2O_4S$  (M + H), 479.1252; found, 479.1236. Analytical HPLC  $t_R = 1.85$  min, 100% pure (A);  $t_R = 2.16$  min, 100% pure (C).

**2-Methyl-2-[4-[(4-methyl-2-[4-(methylsulfonyl)oxy]phenyl]-1,3-thiazol-5-yl)carbonyl]amino]methyl]phenoxy]propanoic Acid (25l).** To a solution of **24l** (0.34 g, 0.64 mmol) in THF (10 mL) was added a solution of LiOH in water (1 equiv, 2.5 mL), and the mixture was stirred at rt for 24 h. The THF was evaporated, and the aqueous phase was acidified with HCl (1 N) and then extracted with ethyl acetate (50 mL). The organic layer was dried over  $Na_2SO_4$ , filtered, and evaporated to dryness. The residue was chromatographed, eluting with  $CH_2Cl_2/MeOH$  95/5 then 90/10 to afford **25l** as a white solid (50 mg, 15%).  $^1H$  NMR (DMSO- $d_6$ )  $\delta$  8.78 (t,  $J=5.8$  Hz, 1H), 8.03 (d,  $J=8.9$  Hz, 2H), 7.48 (d,  $J=8.7$  Hz, 2H), 7.13 (d,  $J=8.7$  Hz, 2H), 6.80 (d,  $J=8.5$  Hz, 2H), 4.33 (d,  $J=5.7$  Hz, 2H), 3.44 (s, 3H), 2.61 (s, 3H), 1.40 (s, 6H). MS (APCI)  $m/z$  505 (M + H)<sup>+</sup>. HRMS calcd for  $C_{23}H_{24}N_2O_7S_2$  (M + H), 505.1103; found, 505.1088. Analytical HPLC  $t_R = 1.59$  min, 100% pure (A);  $t_R = 1.93$  min, 100% pure (C).

**2-[(4-[(2-(4-Hydroxyphenyl)-4-methyl-1,3-thiazol-5-yl)carbonyl]amino)methyl]phenoxy]oxy-2-methylpropanoic Acid (25m).** To a solution of **24l** (0.20 g, 0.38 mmol) in THF (30 mL) and EtOH (5 mL) was added NaOH solution (1 N, 1.85 mL, 5 equiv), and the mixture was stirred at 70 °C for 4 h. The mixture was cooled to room temperature, and the solution was acidified with HCl (1 N) and extracted with ethyl acetate (3 × 50 mL). The combined organic layers were washed with  $H_2O$ , dried over  $Na_2SO_4$ , filtered, and evaporated to dryness. The residue was crystallized in a mixture of  $CH_2Cl_2$  and THF to afford **25m** (0.12 g, 74%) as white crystals; mp 151–152 °C.  $^1H$  NMR (DMSO- $d_6$ ):  $\delta$  13.00 (s, 1H), 10.13 (s, 1H), 8.67 (s, 1H), 7.35 (d,  $J=8.7$  Hz, 2H), 7.21 (d,  $J=8.7$  Hz, 2H), 6.86 (d,  $J=8.7$  Hz, 2H), 6.77 (d,  $J=8.6$  Hz, 2H), 4.33 (d,  $J=5.6$  Hz, 2H), 2.57 (s, 3H), 1.48 (s, 6H). MS (APCI)  $m/z$  427 (M + H)<sup>+</sup>. HRMS calcd for  $C_{22}H_{22}N_2O_5S$  (M + H),

**Table 8.** Data Collection and Refinement Statistics

crystallization	PPAR $\alpha$ /SRC1 peptide <b>25a</b>
PDB code	to be deposited
unit cell dimensions	
<i>a</i> (Å)	61.3
<i>b</i> (Å)	103.5
<i>c</i> (Å)	49.9
space group	<i>P</i> 2 <sub>1</sub> 2 <sub>1</sub> 2
molecules per asymmetric unit	1
resolution (Å)	50–1.8
number of unique reflections	30 145
data redundancy	7.1
completeness (%)	99.4
<i>R</i> <sub>symm</sub> (%)	4.5
<i>I</i> / $\sigma$	39.4
	Refinement
<i>R</i>	20.4
<i>R</i> <sub>free</sub>	22.7
r.m.s. deviation from ideality	
bond length (Å)	0.005
bond angle (degrees)	1.288
average B-factor (Å <sup>2</sup> )	
all atoms	27.0
protein atoms	25.9
water molecules	37.5
ligand	19.7

427.1328; found, 427.1319. Analytical HPLC *t*<sub>R</sub> = 2.06 min, 100% pure (B); *t*<sub>R</sub> = 1.78 min, 98.9% pure (C).

**Ethyl 5-Methyl-2-[4-(trifluoromethyl)phenyl]-1,3-thiazole-4-carboxylate (38).** To a solution of 2-ketobutyric acid (5.0 g, 49 mmol) in CH<sub>2</sub>Cl<sub>2</sub> (10 mL) was slowly added bromine (1 equiv; 2.5 mL), and the mixture was stirred at rt for 15 min. The solvent was evaporated. Toluene was added and the solvent was evaporated again. The residue was dissolved in EtOH, then **1a** (8.5 g; 0.85 equiv) was added, and the mixture was stirred at 80 °C for 18 h. The solvent was evaporated, and the crude product was chromatographed, eluting with CH<sub>2</sub>Cl<sub>2</sub> to afford **38** (4.56 g, 35%) as a white solid. <sup>1</sup>H NMR (CDCl<sub>3</sub>):  $\delta$  8.04 (d, *J* = 8.4 Hz, 2H), 7.68 (d, *J* = 8.1 Hz, 2H), 4.45 (q, *J* = 7.2 Hz, 2H), 2.82 (s, 3H), 1.43 (t, *J* = 7.2 Hz, 3H).

**Protein Preparation.** The PPAR $\alpha$  ligand binding domain (amino acids 192–468) with an N-terminal 6xHis tag was expressed using the T7 promoter of plasmid vector pRSETA. BL21(DE3) *E. coli* cells transformed with this expression vector were grown at 24 °C in shaker flasks for 66 h. The cells were harvested, resuspended, and lysed. The lysed cells were centrifuged, and the supernatant was loaded on a Ni-agarose column. The column was washed with 150 mL of buffer A (10% glycerol, 20 mM HEPES pH 7.5, 25 mM imidazole), and the protein was eluted with a 450 mL gradient of buffer B (10% glycerol, 20 mM HEPES pH 7.5, 500 mM imidazole). The protein, which eluted at 20% buffer B, was diluted with one volume of buffer C (20 mM HEPES, pH 7.5, 1 mM EDTA) and loaded on a 100 mL S-Sepharose (Pharmacia, Peapack, New Jersey) column. The column was washed with 100 mL buffer C, and the PPAR $\alpha$  LBD protein was eluted with a 200 mL gradient of buffer D (20 mM HEPES, pH 7.5, 10 mM DTT, 1 M ammonium acetate). The PPAR $\alpha$  LBD eluted from the column at 43% buffer D. The protein yield was 9 mg/L of cells grown and was >95% pure, as determined by SDS-PAGE analysis.

The protein was then diluted to 1 mg/mL with buffer C such that the final buffer composition was 220 mM ammonium acetate, 20 mM HEPES pH 7.5, 1 mM EDTA, and 1 mM DTT. The peptide SRC1<sup>16</sup> was added in a molar ratio of 1.5 as a 2 mg/100  $\mu$ L DMSO stock. The ligand was then added in a 5:1 molar ratio as a 2 mg/100  $\mu$ L DMSO stock and spun at 4 K for 20 min to clarify the solution before concentrating in Centriprep 10 filtration units (Millipore, Bedford, Massachusetts). The solution containing the PPAR $\alpha$  LBD-SRC1 complexes was concentrated to approximately 10 mg/mL with 80% yield.

**Crystallization and Data Collection.** The crystals were grown at room temperature using the hanging drop vapor diffusion method.

The hanging drops contained 1  $\mu$ L of the above protein–ligand solution and 1  $\mu$ L of well buffer comprising 7% PEG 3350, 200 mM NaF, and 12% 2,5-hexanediol. Crystals formed in the space group *P*2<sub>1</sub>2<sub>1</sub>2 with cell dimensions *a* = 61.3 Å, *b* = 103.5 Å, and *c* = 49.9 Å. Each asymmetric unit contained a single LBD complex with 45% solvent content. X-ray data was collected at the IMCA 17-ID line (Argonne, IL) and processed with HKL2000.<sup>20</sup> Statistics are summarized in Table 8.

**Structure Determination and Refinement.** The structure was determined by molecular replacement methods with the program AmoRe,<sup>21</sup> as implemented in the CCP4 suite.<sup>22</sup> The structure of the PPAR $\alpha$  LBD,<sup>23</sup> residues 167–441, was used as the initial model. The best fitting solution gave a correlation coefficient of 70% and an R-factor of 33%. Model building was performed with the software program QUANTA, and structure refinement was carried out with the CNS software program.<sup>24</sup> Refinement statistics are summarized in Table 8.

**Acknowledgment.** The authors thank Melanie Barnathan and Vanessa Cheminade for valuable technical assistance.

**Supporting Information Available:** Experimental details and data for compounds **3b–k**, **4**, **5**, **6**, **7**, **8**, **9**, **10**, **11**, **12**, **13**, **14**, **15**, **16**, **17b–k**, **18**, **19**, **20**, **21**, **22**, **23**, **24b–j**, **25b–j**, **26**, **27**, **28**, **29**, **30**, **31**, **32**, **33**, **34**, **35**, **36**, **37**, **24k**, **25k**, **24l**, **39**, **40**, **41**, **42**, **43**, **44**, and **45** plus a table of analytical data for target compounds. This material is available free of charge via the Internet at <http://pubs.acs.org>

## References

- Tobert, J. A. Lovastatin and Beyond: The History of the HMG-CoA Reductase Inhibitors. *Nat. Rev. Drug Discovery* **2003**, *2*, 517–526.
- Sprecher, D. L. Raising High-Density Lipoprotein Cholesterol with Niacin and Fibrates: A Comparative Review. *Am. J. Cardiol.* **2000**, *86* (suppl), 46L–50L.
- Rader, D. J. Effects of Nonstatin Lipid Drug Therapy on High-Density Lipoprotein Metabolism. *Am. J. Cardiol.* **2003**, *91* (suppl), 18E–23E.
- Wise, A.; Foord, S. M.; Fraser, N. J.; Barnes, A. A.; Elshourbagy, N.; Eilert, M.; Ignar, D. M.; Murdock, P. R.; Steplewski, K.; Green, A.; Brown, A. J.; Dowell, S. J.; Szekeres, P. G.; Hassall, D. G.; Marshall, F. H.; Wilson, S.; Pike, N. B.; Molecular Identification of High and Low Affinity Receptors for Nicotinic Acid. *J. Biol. Chem.* **2003**, *278*, 9869–9874.
- Issemann, I.; Green, S.; Activation of a member of the steroid hormone receptor superfamily by peroxisome proliferators. *Nature* **1990**, *347*, 645–650.
- Forman, B. M.; Chen, J.; Evans, R. M.; Hypolipidemic drugs, polyunsaturated fatty acids, and eicosanoids are ligands for peroxisome proliferator-activated receptors  $\alpha$  and  $\delta$ . *Proc. Natl. Acad. Sci. U.S.A.* **1997**, *94*, 4312–4317.
- Chawla, A.; Repa, J. J.; Evans, R. M.; Mangelsdorf, D. J.; Nuclear Receptors and Lipid Physiology: Opening the X-Files. *Science* **2001**, *294*, 1866–1870.
- Hertz, R.; Bishara-Shieban, J.; Bar-Tana, J.; Mode of Action of Peroxisome Proliferators as Hypolipidemic Drugs. Suppression of Apolipoprotein C-III. *J. Biol. Chem.* **1995**, *270*, 13470–13475.
- Berthou, L.; Duverger, N.; Emmanuel, F.; Langouet, S.; Auwerx, J.; Guillouzo, A.; Fruchart, J.-C.; Rubin, E.; Denèfle, P.; Staels, B.; Branellec, D.; Opposite Regulation of Human Versus Mouse Apolipoprotein A-1 by Fibrates in Human Apolipoprotein A-1 Transgenic Mice. *J. Clin. Invest.* **1996**, *97*, 2408–2416.
- Willson, T.; Brown, P. J.; Stenbach, D. D.; Henke, B. R. The PPARs: From Orphan Receptors to Drug Discovery. *J. Med. Chem.* **2000**, *43*, 527–550.
- Staels, B.; Dallongeville, J.; Auwerx, J.; Schoonjans, K.; Leitersdorf, E.; Fruchart, J.-C. Mechanism of Action of Fibrates on Lipid and Lipoprotein Metabolism. *Circulation* **1998**, *98*, 2088–2093.
- (a) Xu, Y.; Mayhugh, D.; Saeed, A.; Wang, X.; Thompson, R. C.; Dominianni, S. J.; Kauffman, R. F.; Singh, J.; Bean, J. S.; Bensch, W. R.; Barr, R. J.; Osborne, J.; Montrose-Rafizadeh, C.; Zink, R. W.; Yumibe, N. P.; Huang, N.; Luffer-Atlas, D.; Rungta, D.; Maise, D. E.; Mantlo, N. B. Design and Synthesis of a Potent and Selective Triazolone-Based Peroxisome Proliferator-Activated Receptor  $\alpha$  Agonist. *J. Med. Chem.* **2003**, *46*, 5121–5124. (b) Nomura, M.; Tanase, T.; Ide, T.; Tsunoda, M.; Suzuki, M.; Uchiki, H.; Murakami, K.; Miyachi, H.; Design, Synthesis, and Evaluation of Substituted

- Phenylpropanoic Acid Derivatives as Human Peroxisome Proliferator Activated Receptor Activators. Discovery of Potent and Human Peroxisome Proliferator Activated Receptor  $\alpha$  Subtype-Selective Activators. *J. Med. Chem.* **2003**, *46*, 3581–3599. (c) Brown, P. J.; Winegar, D. A.; Plunket, K. D.; Moore, L. B.; Lewis, M. C.; Wilson, J. G.; Sundseth, S. S.; Koble, C. S.; Wu, Z.; Chapman, J. M.; Lehmann, J. M.; Kliewer, S. A.; Willson, T. M. A Ureido-Thioisobutyric Acid (GW9578) Is a Subtype-Selective PPAR $\alpha$  Agonist with Potent Lipid-Lowering Activity. *J. Med. Chem.* **1999**, *42*, 3785–3788.
- (13) Oliver, W. R.; Shenk, J. L.; Snaith, M. R.; Russell, C. S.; Plunket, L. D.; Bodkin, N. L.; Lewis, M. C.; Winegar, D. A.; Sznajdman, M. L.; Lambert, M. H.; Xu, E.; Sternbach, D. D.; Kliewer, S. A.; Willson, T. M. A Selective Peroxisome Proliferator-Activated Receptor  $\delta$  Agonist Promotes Reverse Cholesterol Transport. *Proc. Natl. Acad. Sci. U.S.A.* **2001**, *98*, 5306–5311.
- (14) Henke, B. R.; Blanchard, S. G.; Brackeen, M. F.; Brown, K. K.; Cobb, J. E.; Collins, J. L.; Harrington, W. W., Jr.; Hashim, M. A.; Hull-Ryde, E. A.; Kaldor, I.; Kliewer, S. A.; Lake, D. H.; Leesnitzer, L. M.; Lehmann, J. M.; Lenhard, J. M.; Orband-Miller, L. A.; Miller, J. F.; Mook, R. A.; Noble, S. A.; Oliver, W.; Parks, D. J.; Plunket, K. D.; Szewczyk, J. R.; Willson, T. M. *N*-(2-Benzoylphenyl)-*L*-tyrosine PPAR $\gamma$  Agonists. 1. Discovery of a Novel Series of Potent Antihyperglycemic and Antihyperlipidemic Agents. *J. Med. Chem.* **1998**, *41*, 5020–5036.
- (15) Xu, H. E.; Lambert, M. H.; Montana, V. G.; Plunket, K. D.; Moore, L. B.; Collins, J. L.; Oplinger, J. A.; Kliewer, S. A.; Gampe, R. T., Jr.; McKee, D. D.; Moore, J. T.; Willson, T. M.; Structural Determinants of Ligand Binding Selectivity between the Peroxisome Proliferator-Activated Receptors. *Proc. Natl. Acad. Sci. U.S.A.* **2001**, *98*, 13919–13924.
- (16) Cronet, P.; Petersen, J. F. W.; Folmer, R.; Blomberg, N.; Sjoblom, K.; Karlsson, U.; Lindstedt, E.-L.; Bamberg, K. Structure of the PPAR $\alpha$  and  $\gamma$  Ligand Binding Domain in Complex with AZ 242; Ligand Selectivity and Agonist Activation in the PPAR Family. *Structure* **2001**, *9*, 699–706.
- (17) Gampe, R. T., Jr.; Montana, V. G.; Lambert, M. H.; Miller, A. B.; Bledsoe, R. K.; Milburn, M. V.; Kliewer, S. A.; Willson, T. M.; Xu, H. E. Asymmetry in the PPAR $\gamma$ /RXR $\alpha$  Crystal Structure Reveals the Molecular Basis of Heterodimerization among Nuclear Receptors. *Mol. Cell* **2000**, *5*, 545–555.
- (18) Takada, I.; Yu, R. T.; Xu, H. E.; Lambert, M. H.; Montana, V. G.; Kliewer, S. A.; Evans, R. M.; Umesono, K. Alteration of a Single Amino Acid in Peroxisome Proliferator-Activated Receptor- $\alpha$  (PPAR $\alpha$ ) Generates a PPAR $\delta$  Phenotype. *Mol. Endocrinol.* **2000**, *14*, 733–740.
- (19) Berthou, L.; Duverger, N.; Emmanuel, F.; Langouet, S.; Auwerx, J.; Guillouzo, A.; Fruchart, J. C.; Rubin, E.; Deneffe, P.; Staels, B.; Branellex, D. Opposite Regulation of Human Versus Mouse Apolipoprotein A-I by Fibrates in Human Apolipoprotein A-I Transgenic Mice. *J. Clin. Invest.* **1996**, *97*, 2408–2416.
- (20) Otwinowski, Z.; Minor, W. Macromolecular Crystallography, Part A. In *Methods in Enzymology*; Carter, C. W., Jr., Sweet, R. M., Eds.; Academic Press: New York, 1997; Vol. 276, pp 307–326.
- (21) Navaza, J. *AMoRe*: An Automated Package for Molecular Replacement. *Acta Crystallogr.* **1994**, *A50*, 157–163.
- (22) Collaborative Computational Project, Number 4. “The CCP4 Suite: Programs for Protein Crystallography”. *Acta Crystallogr.* **1994**, *D50*, 760–763.
- (23) Xu, H. E.; Lambert, M. H.; Montana, V. G.; Parks, D. J.; Blanchard, S. G.; Brown, P. J.; Sternbach, D. D.; Lehmann, J. M.; Wisely, G. B.; Willson, T. M.; Kliewer, S. A.; Milburn, M. V. Molecular Recognition of Fatty Acids by Peroxisome Proliferator-Activated Receptors. *Mol. Cell* **1999**, *3*, 397–403.
- (24) Brünger, A. T.; Adams, P. D.; Clore, G. M.; DeLano, W. L.; Gros, P.; Grosse-Kunstleve, R. W.; Jiang, J.-S.; Kuszewski, J.; Nilges, M.; Pannu, N. S.; Read, R. J.; Rice, L. M.; Simonson, T.; Warren, G. L. Crystallography and NMR System: A New Software Suite for Macromolecular Structure Determination. *Acta Crystallogr.* **1998**, *D54*, 905–921.

JM058056X